Akademie věd České republiky
Ústav teorie informace a automatizace, v.v.i.

Academy of Sciences of the Czech Republic
Institute of Information Theory and Automation

# RESEARCH REPORT

Ondřej Tichý, Václav Šmídl

## Convolution Model of Time-activity Curves in Blind Source Separation

No. 2330 April 11, 2013

**GAČR No. 13-29225S**

ÚTIA AV ČR, P.O.Box 18, 182 08 Prague, Czech Republic
Tel: (+420)266052422, Fax: (+420)286890378, Url: http://www.utia.cas.cz, E-mail: utia@utia.cas.cz

This report presents a draft of a manuscript, which is intended to be submitted for publication. Any opinions and conclusions expressed in this report are those of the authors and do not necessarily represent the views of the involved institutions.

**Abstract**

Availability of input and organ functions is a prerequisite for analysis of dynamic image sequences in scintigraphy and positron emission tomography (PET) via kinetic models. In PET, the input function can be directly measured by sampling the arterial blood. This invasive procedure can be substituted by extraction of the input function from the observed images. Standard procedure for the extraction is based on manual selection of a region of interest (ROI) which is user-dependent and inaccurate. The aim of our contribution is to demonstrate a new procedure for simultaneous estimation of the input and organ functions from the observed image sequence. We design a mathematical model that integrates all common assumption of the domain, including convolution of the input function and tissue-specific kernels. The input function as well as the kernel parameters are considered to be unknown. They are estimated from the observed images using the Variational Bayes method. The ability of the resulting algorithm to extract the input function is tested on data from dynamic renal scintigraphy. The estimated input function was compared with the common estimate based on manual selection of the heart ROI.

# 1 Introduction

Decomposition of the observed sequences of images into tissue images and their associated time-activity curves (TACs) is a common task in nuclear medicine in scintigraphy or positron emission tomography (PET). The knowledge of the input function is often necessary for further analysis [17, 19]. For example, the input function is essential in the Patlak-Rutland plot [13]. The input function is often associated with the time activity curve of the blood, hence it can be measured from samples of the arterial blood [10]. This approach needs medical intervention which is often not appropriate in clinical practice. Non-invasive estimation of the input function is often done by using manual selection of a regions of interest (ROIs) on appropriate regions of the observed images. It can be placed directly on the heart, if available, or on other vascular structures if they can be recognized on the images [9]. The disadvantages of manual selection of the ROIs are substantial: the position of ROIs is strongly operator-dependent and very time-consuming [4, 3]. Moreover, it is possible that the selected ROI does not contain only the vascular activity but also other tissues in the background.

Automatic, or semi-automatic methods for ROI selection are available [8, 16], however, they are not completely reliable and the activity is always counted from the full area of ROI which may still include some background organs. An alternative approach is to use some blind source separation method (BSS). In their basic form, they do not contain any assumption of convolution, [12], however, such extensions have also been proposed [5, 15]. Based on these ideas, we propose an alternative model tailored for the considered application in nuclear imaging. In the model, the tissue images, tissue TACs, and the input function are considered unknown and are automatically estimated from the image se-

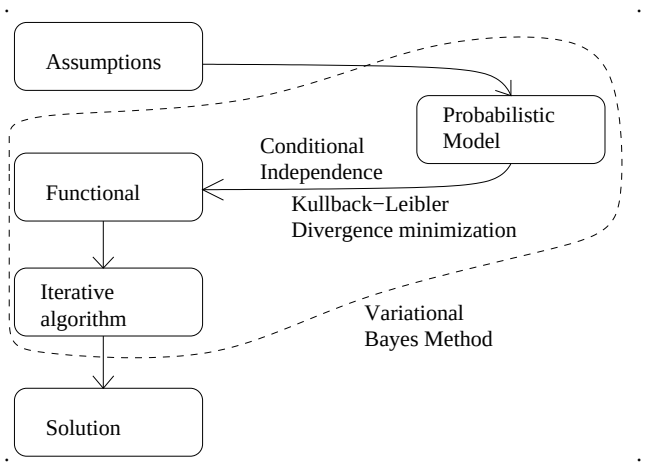


Figure 1: The scheme of the Variational Bayes method.

quence. We will show that the estimation is possible and provides meaningful results on the clinical data.

# 2 Mathematical Model

The goal of the designed method is to automatically identify tissue structures and their related time-activity curves (TACs) and their decomposition from the observed sequence of images. Estimation procedure is based on probabilistic model that is designed using common assumptions used in nuclear medicine. These assumptions are: (i) the observed image is a superposition of the underlying tissue images; (ii) the time activity curves are described by compartment model, each time-activity curve arise as a convolution between a common input function and a tissue-specific kernel [15]; (iii) the tissue images and the time activity curves are non-negative; and (iv) the variance of the observation noise is proportional to the signal strength. These assumption are now formulated mathematically via a probabilistic model. The Variational Bayes methodology, see Fig. 1, is used to estimate all unknown parameters of the proposed model.

## 2.1 Deterministic Formulation

The observed sequence of images is indexed by a discrete time index $t$, the number of images in the sequence is assumed to be $n$. The sequence is assumed to be composed of $r$ underlying tissues indexed by symbol $f = 1, \ldots, r$ , the number $r$ is unknown and should be estimated during the estimative procedure. Each observed image is stored in vector $\mathbf{d}_t$ where the pixels are stored columnwise and $\mathbf{d}_t$ is assumed to be a sum of contributions from the underlying tissues in

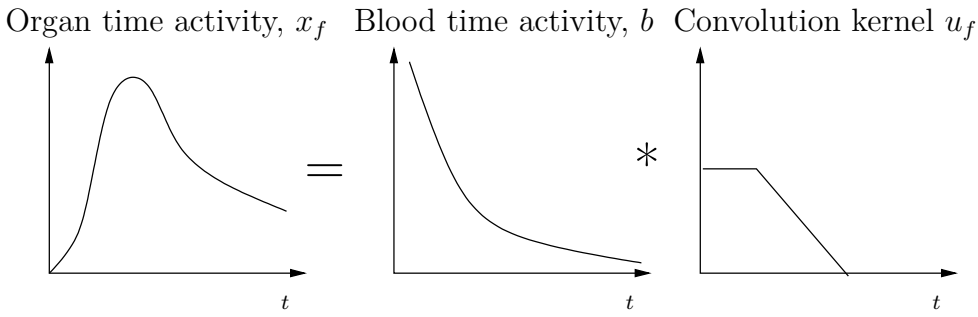


Figure 2: Illustration of the assumed shape of the convolution kernels.

sense of superposition as

$$\mathbf{d}_t = \sum_{f=1}^{r} \mathbf{a}_f x_{t,f}, \tag{1}$$

where $\mathbf{a}_f$ are the tissue images in the same vector form as the observed image, and $x_{t,f}$ is the activity of the $f$th tissue at time $t$. The time-activity curve $\mathbf{x}_f$, i.e. the organ function, is supposed be the result of convolution of the common input function, $\mathbf{b}$, and a tissue-specific kernel, $\mathbf{u}_f$, see Fig. 2, which can be written discretely as

$$\mathbf{x}_{t,f} = \sum_{i=1}^{t} b_{t-i+1} u_{i,f}, \tag{2}$$

The tissue-specific kernels, $\mathbf{u}_f$ are modeled using increments $\mathbf{w}_f$ as proposed in [11], hence

$$u_{t,f} = \sum_{i=t}^{n} w_{i,f}, \tag{3}$$

Here, $\mathbf{w}_f$ is the $f$th tissue-specific vector with non-negative elements which are assumed to have cluster structure. We propose the following definition

$$w_{i,f} = \begin{cases} h_f & s_f \leq t \leq s_f + l_f, \\ 0 & \text{otherwise}, \end{cases} \tag{4}$$

where, $h_f$ is the height of each increment in $f$th tissue, $s_f$ is the starting point of the increments and $s_f + l_f$ is the ending point of the increments, see Fig. 3 for clarity. In other words, the vector $\mathbf{w}_f$ is supposed to be in the form of $[0, \ldots, 0, h_f, \ldots, h_f, 0, \ldots, 0] \equiv M_{w_f}$.

The input function $\mathbf{b}_t$ is also modeled incrementally using vector $\mathbf{g}$, $\mathbf{g}_i$ are increments of the input function as

$$\mathbf{b}_t = \sum_{i=t}^{n} g_i. \tag{5}$$

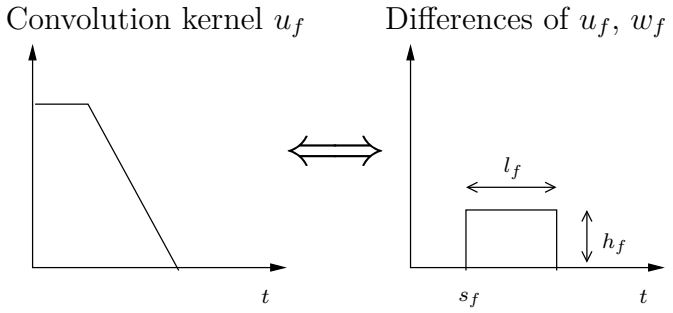


Figure 3: Parametrization of the convolution kernel via differences.

## 2.2 Probabilistic Formulation

The deterministic model assumptions in Section 2.1 are valid only approximately. For example, the measurements of $\mathbf{d}_t$ (1) are subject to noise with unknown variance $\omega$. The observed images $\mathbf{d}_t$ are thus random realizations from the probability density:

$$f(\mathbf{d}_t|\omega) = \mathrm{tN}(\sum_{f=1}^{r} \mathbf{a}_f x_{t,f}, \omega^{-1} I_p), \tag{6}$$

where $p$ denotes the number of pixels in the image, $I_n$ is the identity matrix of size $n$, $\mathrm{tN}(.,.)$ is the multivariate normal distribution truncated to positive values with given mean vector and covariance matrix. Following the Bayesian approach, each unknown parameter needs to have a prior distribution of its potential values. The prior distribution of the unknown variance of the observation noise, $\omega$, is assumed to be of the gamma form,

$$f(\omega) = \mathrm{G}_\omega(\vartheta_0, \rho_0), \tag{7}$$

with prior parameters $\vartheta_0, \rho_0$.

The convolution kernel (2) may also differ from the assumed form, where the variances of the differences are unknown, denoted $\xi_f$ . The model of the TACs is composed from the kernels $\mathbf{w}_f$ and the input function $\mathbf{b}$. The prior distribution of the $f$th TAC model is then

$$\begin{aligned}
f(\mathbf{w}_f|\xi_f) &= \mathrm{tN}(M_{w_f}, \xi_f I_n), && (8)\\
f(\xi_f) &= \mathrm{G}(\kappa_{f,0}, \nu_{f,0}), && (9)\\
f(h_f) &= \mathrm{tN}(\mathbf{0}_{r\times 1}, \tau_0), && (10)\\
f(l_f|s_f) &= \mathrm{U}(0, n - s_f), && (11)\\
f(s_f) &= \mathrm{U}(0, n), && (12)
\end{aligned}$$

where the parameters indexed with zero are assumed to be known prior parameters, and $\mathrm{U}(.,.)$ is the uniform distribution.

Since (5) models a straight line, the true input function must differ from it. The variance of the differences between the true input function and the model (5) is assumed to have unknown variance $\psi$. The prior distribution for the parameters of the input function is

$$f(\mathbf{g}|\psi) = \mathrm{tN}(\mathbf{0}_{n\times 1}, \psi^{-1} I_n), \tag{13}$$
$$f(\psi) = \mathrm{G}(\zeta_0, \eta_0), \tag{14}$$

with prior parameters $\zeta_0, \eta_0$.

The model of tissue images is assumed to be

$$f(\mathbf{a}_f|\upsilon_f) = \mathrm{tN}(\mathbf{0}_{p\times 1}, \upsilon_f^{-1} I_p), \tag{15}$$
$$f(\upsilon_f) = \mathrm{G}(\alpha_{f,0}, \beta_{f,0}). \tag{16}$$

Here, $\upsilon_f$ is a hyperparameter that allows to select the number of relevant tissue images, $r$, via the automatic relevance determination approach (ARD), [1].

In further text, this model will be denoted as the Blind Compartment Model Separation (BCMS).

## 2.3 Implicit Solution of the Model

Note that we switch from the vector notation the the matrix one for simplification. Then, each matrix is composed from respected vectors as its columns such as $A = [\mathbf{a}_1, \ldots, \mathbf{a}_r]$. Following the Variational Bayes method [18], the optimal approximative posterior densities were identified to be:

$$\tilde{f}(\mathbf{g}|D, r) = \mathrm{tN}(\mu_{\mathbf{g}}, \Sigma_{\mathbf{g}}), \qquad \tilde{f}(\psi|D, r) = \mathrm{G}(\zeta, \eta), \tag{17}$$
$$\tilde{f}(\mathrm{vect}(W)|D, r) = \mathrm{tN}(\mu_{\mathrm{vect}(W)}, \Sigma_{\mathrm{vect}(W)}), \qquad \tilde{f}(\xi_f|D, r) = \mathrm{G}(\kappa_f, \nu_f), \tag{18}$$
$$\tilde{f}(A|D, r) = \mathrm{tN}(\mu_A, I_p \otimes \Phi_A), \qquad \tilde{f}(\upsilon_f|D, r) = \mathrm{G}(\alpha_f, \beta_f), \tag{19}$$
$$\tilde{f}(\omega|D, r) = \mathrm{G}_\omega(\vartheta, \rho). \tag{20}$$

Note that vectorized form of matrix $W$, $\mathrm{vect}(W)$, has to be used for computation reason. Shaping parameters $\mu_{\mathbf{g}}, \Sigma_{\mathbf{g}}, \zeta, \eta, \mu_{\mathrm{vect}(W)}, \Sigma_{\mathrm{vect}(W)}, \kappa_f, \nu_f, \mu_A, \Phi_A, \alpha_f, \beta_f, \vartheta, \rho$ are computed and lead to the following set of implicit equations:

$$\Phi_A = (\widehat{\omega X'X} + \widehat{\Upsilon})^{-1}, \tag{21}$$

$$\mu_A = (\widehat{\omega} D \widehat{X}) \Phi_A, \tag{22}$$

$$\Sigma_g = (\widehat{\psi} I_n)^{-1}, \tag{23}$$

$$\mu_g = \Sigma_g C' \sum_{i=1}^{r} \Big( \Big( \sum_{k=0}^{n-1} \Delta_k' \widehat{u_{k+1,i}} \Big) D' \widehat{a}_i \Big), \tag{24}$$

$$\Sigma_{\mathrm{vect}(W)} = \Big( ((\widehat{A'A})' \otimes \widehat{\omega} C' \widehat{B'B} C) + (\widehat{\Xi_W} \otimes I_n) \Big)^{-1}, \tag{25}$$

$$\mu_{\mathrm{vect}(W)} = \Sigma_{\mathrm{vect}(W)} \left( \widehat{\Xi_W} \mathrm{vect}((C' \widehat{B'B} C)^{-1} C' \widehat{B}' D' \widehat{A} (\widehat{A'A})^{-1}) + (\widehat{\Xi_W} \otimes I_n) \mathrm{vect}(\widehat{M_W}) \right), \tag{26}$$

$$\nu = \nu_0 + \frac{1}{2} \mathrm{diag}(\widehat{W'W}) + \frac{1}{2} \mathrm{diag}(-2 \widehat{W}' \widehat{M_W}) + \frac{1}{2} \mathrm{diag}(\widehat{M_W' M_W}), \tag{27}$$

$$\rho = \rho_0 + \frac{1}{2} \mathrm{tr}(DD' - 2 \widehat{A} \widehat{X}' D') + \frac{1}{2} \mathrm{tr}\Big( \widehat{AX'XA'} \Big), \tag{28}$$

$$\alpha = \alpha_0 + \frac{p}{2} \mathbf{1}_{r,1}, \tag{29}$$

$$\beta = \beta_0 + \frac{1}{2} \mathrm{diag}(\widehat{A'A}), \tag{30}$$

$$\kappa = \kappa_0 + \frac{n}{2} \mathbf{1}_{r,1}, \tag{31}$$

$$\zeta = \zeta_0 + \frac{n}{2}, \tag{32}$$

$$\eta = \eta_0 + \frac{1}{2} \mathrm{tr}(\widehat{\mathbf{g}'\mathbf{g}}), \tag{33}$$

$$\vartheta = \vartheta_0 + \frac{np}{2}. \tag{34}$$

Here, $\hat{x}$ denotes estimate of variable $x$, $\otimes$ denotes the Kronecker product, $M_W$ contains a prior vectors of $W$ composed of estimates of $h$, $s$, and $l$ (obtained using EM algorithm [6]), auxiliary matrix $\Delta_k \in \mathbf{R}^{n \times n}$ is defined as $(\Delta_k)_{i,j} = \begin{cases} 1, & \text{if } i - j = k, \\ 0, & \text{otherwise,} \end{cases}$, and auxiliary matrix $C \in \mathbf{R}^{n \times n}$ is defined as

$$C = \begin{pmatrix} 1 & 1 & \dots & 1 & 1 \\ 0 & 1 & \dots & 1 & 1 \\ \vdots & \vdots & \ddots & \vdots & \vdots \\ 0 & 0 & \dots & 0 & 1 \end{pmatrix}. \tag{35}$$

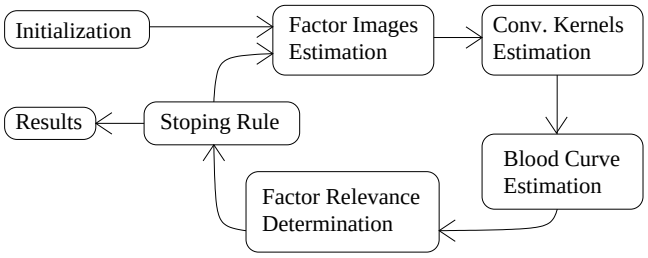


Figure 4: The scheme of the BCMS algorithm.

The matrix $B$ consists of elements of blood vector $b$ as follows

$$B = \begin{pmatrix} b_1 & 0 & \cdots & 0 \\ b_2 & b_1 & \cdots & 0 \\ \vdots & \vdots & \ddots & \vdots \\ b_t & b_{t-1} & \cdots & b_1 \end{pmatrix}. \tag{36}$$

The required moments $\widehat{\psi}$, $\widehat{\omega}$, $\widehat{\Upsilon}$, and $\widehat{\Xi_W}$, are computed according to the Appendix A.3 as

$$\widehat{\psi} = \frac{\zeta}{\eta}, \tag{37}$$

$$\widehat{\omega} = \frac{\vartheta}{\rho}, \tag{38}$$

$$\widehat{\Upsilon} = \mathrm{diag}(\alpha \circ \beta^{-1}), \tag{39}$$

$$\widehat{\Xi_W} = \mathrm{diag}(\kappa \circ \nu^{-1}), \tag{40}$$

where symbol $\circ$ denotes Hadamard product. The moments of the normal distributions are computed according to the Appendix A.1 and A.2.

## 2.4 Iterative Solution of the Model

In Section 2.3, we established the set of implicit equations (21) - (40). Following the Variational Bayes method [18], see Fig. 1, the set is solved using iterative algorithm. The scheme of the algorithm can be seen in Fig. 4. Selection of the initialization data is depend on field of use. Note, that our initialization data are selected for use in renal scintigraphy.

The initialization step consists of two main blocks, setting prior parameters and setting the starting data. The prior parameters are selected as follows:

$$\begin{aligned} &\alpha_0 = 10^{-2}, \quad \beta_0 = 10^{-2}, \quad \zeta_0 = 10^{-7}, \quad \eta_0 = 10^{-7}, \quad \kappa_0 = 10^{-2}, \\ &\vartheta_0 = 10^{-2}, \quad \rho_0 = 10^{-2}, \quad \nu_0 = 10^{-2}, \quad \tau_0 = 10^{2}, \quad \varsigma_0 = 10^{10}, \end{aligned}$$

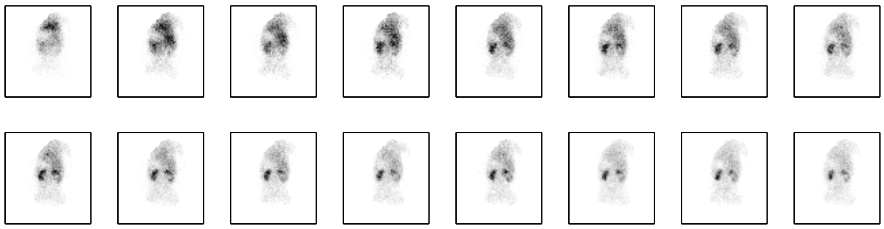

Figure 5: Selected sequence from renal scintigraphy.

to cover the behavior of the data.

The starting data can be selected using the knowledge of the behavior of radiopharmaceuticals and physiological processes in human body. Hence, the initialization of the blood vector $b$ is selected as declining exponential function,

$$\mathbf{b}_{\text{init},j} = \exp\left(-\frac{j}{3}\right), \quad j \in \{1, \ldots, n\}, \tag{41}$$

which corresponds well with physiological assumptions. Then, vectors with tissue-specific kernels can be easily selected as typical kernels related to the task. In case of the renal scintigraphy, we select the typical kernels of: blood, parenchyma, pelves, tissue background (liver and spleen at most), and urinary bladder. It is wise to select more than this structures as the starting point, selection of a few structures cover the whole time of sequence is required.

# 3 Results

We apply the BCMS algorithm from section 2 on a dataset from renal scintigraphy. Since the proposed model is suitable for the datasets where all tissues are activated from the beginning of the measurement, we apply the algorithm on a selected part of the sequence.

## 3.1 Motivation

The motivation for selection of specific part of sequence is that relative renal function (RRF) [2, 14] can be computed on it. Let us describe the basic information about a kidney and the RRF.

A healthy kidney is composed of a parenchyma, spongy tissue covering the whole kidney, and a pelvis, small structure serving to drain the urine from the kidney. The biological fact is that the parenchyma is activated directly from the blood in contrary to the pelvis, which is activated from the parenchyma with delay approximately $100 - 180$ seconds [7]. This time delay is called the uptake time. From this part of sequence and properly separated parenchyma images and TACs, RRF can be estimated. RRF is a percentage of function of the left kidney and the right kidney. The RRF is estimated from the sum

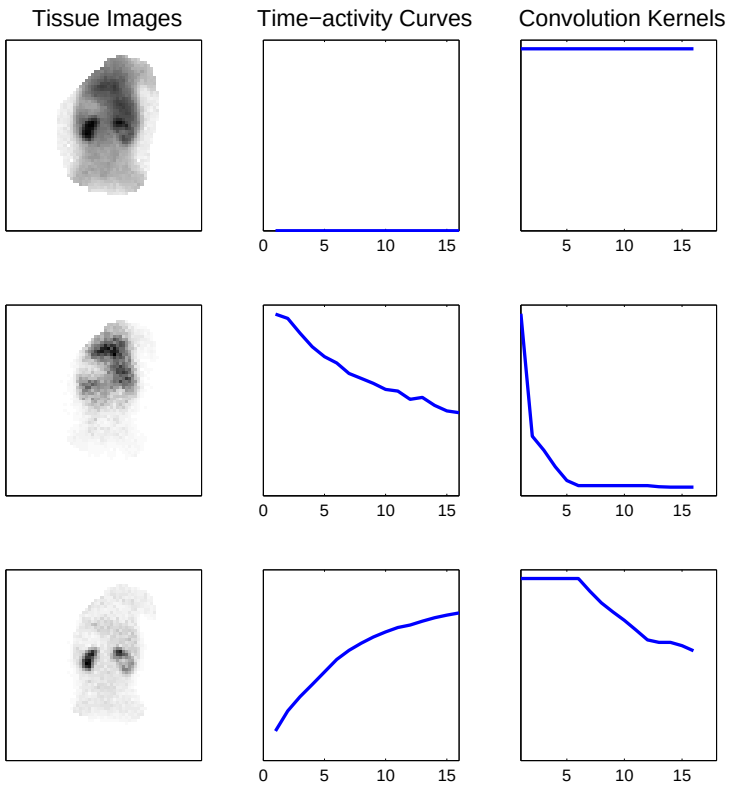


Figure 6: Estimates provided by the BCMS algorithm for a selected dataset. **Left**: estimated tissue images; **middle**: estimated time-activity curve; **right**: estimated tissue-specific kernel.

of activity in the left (L) and in the right (R) parenchyma during the uptake time. Then, $RRF_L = \frac{L}{L+R} \times 100$ % and $RRF_R$ can be computed analogically, both weighted by their time activity curves. Historically, the activity is taken only from the uptake time. The RRF is mainly used in investigation of diseases such as urinary obstruction, renal artery stenosis, renovascular hypertension, pelvi-uretric junction, renal transplant, etc.

## 3.2 Experiment

For experiment, we select the uptake part of the child dataset, see Figure 5. The sequence consist of 16 images, i.e. $n = 16$, of the resolution $64 \times 64$, i.e. $p = 4096$. We select the starting number of tissues as $r = 3$ since we assume

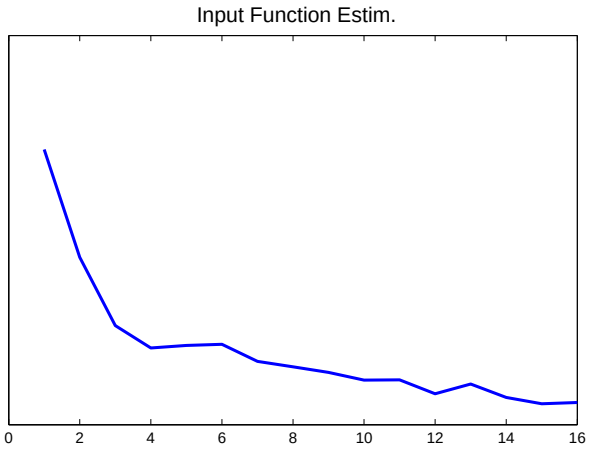


Figure 7: The estimated input function from selected dataset.

that uptake part of the sequence includes two main tissues, parenchyma and tissue background, and the third factor is set for anything that can appear. The algorithm runs till the parameter $\omega$ is stabilized.

The results can be seen in Figure 6. The BCMS algorithm provides results in the form of tissue images, $\mathbf{a}_f$, tissue-specific convolution kernel, $\mathbf{u}_f$, and input function, $\mathbf{b}$. The TACs can be directly computed from the estimates of $\mathbf{u}_f$ and $\mathbf{b}$. The estimates corresponding to the tissue background are displayed in the second row, those corresponding to the parenchyma in the third row. In the first row, it can be seen the estimates with zeros activity, i.e. the dummy factor. Hence, it can be seen that the BCMS algorithm detected only two meaningful tissues. The estimated input function of this dataset is displayed in Figure 7.

The results provided by the BCMS algorithm well correspond to the physiological assumption and are reliable.

# 4 Conclusion

The probabilistic model of Blind Source Separation was proposed in this paper. The key novelty is modeling the time activity curves as the convolution between tissue-specific kernel and common input function, both unknown. The model is solved using the Variational Bayes method and the Blind Compartment Model Separation is established. The results are achieved with no manual intervention. Since the model of convolution kernel is too restrictive, we apply the BCMS algorithm not on the whole sequence but on the uptake part of a sequence. This part of a sequence is crucial e.g. for relative renal function estimation.

On the example run, we show that the estimates of the BCMS algorithm are in consent with physiological expectation. The assumptions of the model

are not unique to scintigraphy, hence the resulting algorithm can be applied in other modality.

**Acknowledgment**

This work was supported by the Czech Science Foundation, grant No. 13-29225S.

# A Probabilistic Distributions

## A.1 Matrix Normal Distribution

Let us assume the matrix $X \in \mathbf{R}^{n\times p}$. The matrix normal distribution of the matrix $X$ is given as

$$N_X(\mu_X, \Sigma_n \otimes \Phi_p) = (2\pi)^{-\frac{np}{2}} |\Sigma_n|^{-\frac{p}{2}} |\Phi_p|^{-\frac{n}{2}} \times \\ \times \exp\left(-\frac{1}{2}\mathrm{tr}\left[\Sigma_n^{-1}(X-\mu_X)(\Phi_p^{-1})'(X-\mu_X)'\right]\right), \quad (42)$$

where $\Sigma_n \in \mathbf{R}^{n\times n}$ and $\Phi_p \in \mathbf{R}^{p\times p}$ are positive definite symmetric matrices, tr() denotes trace of matrix, and $\otimes$ is Kronecker product. Moments of the matrix normal distribution are given as

$$\widehat{X} = \mu_X, \quad (43)$$

$$\widehat{X'X} = \mathrm{tr}(\Sigma_n)\Phi_p + \mu_X{}'\mu_X, \quad (44)$$

$$\widehat{XX'} = \mathrm{tr}(\Phi_p)\Sigma_n + \mu_X\mu_X{}'. \quad (45)$$

Moreover, for $C \in \mathbf{R}^{n\times n}$ and $D \in \mathbf{R}^{p\times p}$ hold following equalities:

$$CXD \sim N(C\mu_X D, C\Sigma_n C' \otimes D'\Phi_p D), \quad (46)$$

$$E(X'DX) = \mu_X' D\mu_X + \mathrm{tr}(\Sigma_n D)\Phi_p, \quad (47)$$

$$E(XCX') = \mu_X C\mu_X' + \Sigma_n \mathrm{tr}(C\Phi_p). \quad (48)$$

## A.2 Truncated Normal Distribution

Truncated normal distribution is defined for scalar random variable $x = N_x(\mu, \sigma)$ on interval $a < x \leq b$ as follows:

$$\mathrm{tN}_x(x|\mu,\sigma,a,b) = \frac{\sqrt{2}\exp((x-\mu)^2)}{\sqrt{\pi}\sigma(erf(\beta)-erf(\alpha))}\chi_{(a;b]}(x), \quad (49)$$

where $\alpha = \frac{a-\mu}{\sqrt{2\sigma}}$, $\beta = \frac{b-\mu}{\sqrt{2\sigma}}$, $\chi_{(a,b]}(x)$ is a characteristic function of interval $(a, b]$ defined as $\chi_{(a,b]}(x) = \begin{cases} 1 & x \in (a, b] \\ 0 & x \notin (a, b] \end{cases}$, and $\mathrm{erf}(t) = \frac{2}{\sqrt{\pi}} \int_0^t e^{-u^2} \mathrm{d}\mathrm{d}u$.

Moments of the truncated normal distribution are given as

$$\widehat{x} = \mu - \sqrt{\sigma} \frac{\sqrt{2}[\exp(-\beta^2) - \exp(-\alpha^2)]}{\sqrt{\pi}(erf(\beta) - erf(\alpha))} \tag{50}$$

$$\widehat{x^2} = \sigma + \mu\widehat{x} - \sqrt{\sigma} \frac{\sqrt{2}[b\exp(-\beta^2) - a\exp(-\alpha^2)]}{\sqrt{\pi}(erf(\beta) - erf(\alpha))}\,. \tag{51}$$

### A.3 Gamma Distribution

The gamma distribution of a random scalar variable $x$ is defined as

$$\mathrm{G}_x(a, b) = \frac{1}{\Gamma(a)} \frac{1}{b^{-a}} x^{a-1} e^{-xb} \tag{52}$$

for $x, a, b > 0$ and $\Gamma(x) = \int_0^\infty t^{x-1} \exp(-t)\, \mathrm{d}\mathrm{d}t$ for $x > 0$.

Moments of the gamma distribution are given as

$$\widehat{x} = \frac{a}{b}, \tag{53}$$

$$\widehat{x^2} = \frac{a}{b^2}. \tag{54}$$

## References


[1] C.M. Bishop and M.E. Tipping. Variational relevance vector machines. In *Proceedings of the 16th Conference on Uncertainty in Artificial Intelligence*, pages 46–53, 2000.

[2] M.D. Blaufox, M. Aurell, B. Bubeck, E. Fommei, A. Piepsz, C. Russell, A. Taylor, H.S. Thomsen, D. Volterrani, et al. Report of the radionuclides in nephrourology committee on renal clearance. *Journal of nuclear medicine: official publication, Society of Nuclear Medicine*, 37(11):1883, 1996.

[3] A. Brink, M. Šámal, and M.D. Mann. The reproducibility of measurements of differential renal function in paediatric 99mtc-mag3 renography. *Nuclear medicine communications*, 33(8):824–831, 2012.

[4] M. Caglar, G.K. Gedik, and E. Karabulut. Differential renal function estimation by dynamic renal scintigraphy: influence of background definition and radiopharmaceutical. *Nuclear medicine communications*, 29(11):1002, 2008.

[5] L. Chen, P.L. Choyke, T.H. Chan, C.Y. Chi, G. Wang, and Y. Wang. Tissue-specific compartmental analysis for dynamic contrast-enhanced mr imaging of complex tumors. *IEEE Transactions on Medical Imaging*, 30(12):2044–2058, 2011.

[6] A.P. Dempster, N.M. Laird, D.B. Rubin, et al. Maximum likelihood from incomplete data via the EM algorithm. *Journal of the Royal Statistical Society*, 39(1):1–38, 1977.

[7] E. Durand, M.D. Blaufox, K.E. Britton, O. Carlsen, P. Cosgriff, E. Fine, J. Fleming, C. Nimmon, A. Piepsz, A. Prigent, et al. International Scientific Committee of Radionuclides in Nephrourology (ISCORN) consensus on renal transit time measurements. In *Seminars in nuclear medicine*, volume 38, pages 82–102. Elsevier, 2008.

[8] E.V. Garcia, R. Folks, S. Pak, and A. Taylor. Totally automatic definition of renal regions-of-interest from tc-99m mag3 renograms: Validation in patients with normal kidneys and in patients with suspected renal obstruction. *Nuclear medicine communications*, 31(5):366, 2010.

[9] G. Germano, B.C. Chen, et al. Use of the abdominal aorta for arterial input function determination in hepatic and renal pet studies. *Journal of nuclear medicine*, 33(4):613, 1992.

[10] H.N.J.M. Greuter, R. Boellaard, et al. Measurement of 18f-fdg concentrations in blood samples: comparison of direct calibration and standard solution methods. *Journal of nuclear medicine technology*, 31(4):206–209, 2003.

[11] A. Kuruc, JH Caldicott, and S. Treves. Improved Deconvolution Technique for the Calculation of Renal Retention Functions. *COMP. AND BIOMED. RES.*, 15(1):46–56, 1982.

[12] J.W. Miskin. *Ensemble learning for independent component analysis*. PhD thesis, University of Cambridge, 2000.

[13] C.S. Patlak, R.G. Blasberg, J.D. Fenstermacher, et al. Graphical evaluation of blood-to-brain transfer constants from multiple-time uptake data. *J Cereb Blood Flow Metab*, 3(1):1–7, 1983.

[14] A. Prigent and P. Cosgriff. Consensus report on quality control of quantitative measurements of renal function obtained from the renogram: International consensus committee from the scientific committee of radionuclides in nephrourology. In *Seminars in nuclear medicine*, volume 29, pages 146–159. Elsevier, 1999.

[15] D.Y. Riabkov and E.V.R. Di Bella. Estimation of kinetic parameters without input functions: analysis of three methods for multichannel blind identification. *Biomedical Engineering, IEEE Transactions on*, 49(11):1318–1327, 2002.

[16] M. Šámal, C.C. Nimmon, K.E. Britton, and H. Bergmann. Relative renal uptake and transit time measurements using functional factor images and fuzzy regions of interest. *European Journal of Nuclear Medicine and Molecular Imaging*, 25(1):48–54, 1997.

[17] D. Vriens, L.F. de Geus-Oei, W.J.G. Oyen, and E.P. Visser. A curve-fitting approach to estimate the arterial plasma input function for the assessment of glucose metabolic rate and response to treatment. *Journal of Nuclear Medicine*, 50(12):1933–1939, 2009.

[18] V. Šmídl and A. Quinn. *The Variational Bayes Method in Signal Processing*. Springer, 2006.

[19] P. Zanotti-Fregonara, R. Maroy, M.A. Peyronneau, R. Trebossen, and M. Bottlaender. Minimally invasive input function for 2-18 f-fluoro-a-85380 brain pet studies. *European journal of nuclear medicine and molecular imaging*, pages 1–9, 2012.